Campos, Rocío; Barrios, Icíar; Lillo, Javier

**Article**

# Experimental CO2 injection: Study of physical changes in sandstone porous media using Hg porosimetry and 3D pore network models

Energy Reports

**Provided in Cooperation with:**
Elsevier

*Suggested Citation:* Campos, Rocío; Barrios, Icíar; Lillo, Javier (2015) : Experimental CO2 injection: Study of physical changes in sandstone porous media using Hg porosimetry and 3D pore network models, Energy Reports, ISSN 2352-4847, Elsevier, Amsterdam, Vol. 1, pp. 71-79,
https://doi.org/10.1016/j.egyr.2015.01.004

Energy Reports 1 (2015) 71–79

Contents lists available at ScienceDirect

Energy Reports

journal homepage: www.elsevier.com/locate/egyr

# Experimental $CO_2$ injection: Study of physical changes in sandstone porous media using Hg porosimetry and 3D pore network models

Rocío Campos [a,*], Icíar Barrios [a], Javier Lillo [b,c]

[a] Laboratorio de Petrofísica, Departamento de Medio Ambiente, CIEMAT. Av. de la Complutense 40, 28040 Madrid, Spain

[b] Departamento de Geología y Biología, Universidad Rey Juan Carlos, Tulipán s/n, Móstoles, 28933 Madrid, Spain

[c] Instituto IMDEA Agua, Punto Net 4, 28805 Alcalá de Henares, Spain

ARTICLE INFO

*Article history:*
Received 23 October 2014
Received in revised form
14 January 2015
Accepted 20 January 2015
Available online 2 March 2015

*Keywords:*
$CO_2$ injection
Sandstones
Porosity

ABSTRACT

Variations in the pore system of sandstones from the so-called Utrillas Formation (Lower Cretaceous, Iberian Peninsula) after $CO_2$ injection have been investigated in a laboratory on a micro scale. In this study, we present results regarding variations in the pore spaces of sandstones caused by the injection of $CO_2$ and its permanence in supercritical conditions in contact with a rock sample for two months. The modifications produced in the porosity and pore size distribution have been evaluated on two geological samples, using a 3D modelling of the results obtained by Hg intrusion porosimetry. Reconstructions of the pore structure of the rock before and after $CO_2$ injection from mercury intrusion–extrusion curves, generating virtual models of pores that reproduce the experimental porosity. By analysing the results, a drastic modification in the mesoporosity of the rock is confirmed, which may have a paramount influence not only on the total storage capacity but also on the percolation of fluid through the rock.



## 1. Introduction

Deep geological storage of $CO_2$ is a promising option to mitigate greenhouse gas emissions in the atmosphere (Pacala and Socolow, 2004). The most favourable sites for the definitive storage of $CO_2$ in the Iberian Peninsula are deep saline aquifers. Considering this option the Mesozoic basement of the Duero Basin (central Spain) includes some of the most promising rock formations for $CO_2$ storage. Currently, there are several projects under way in this sedimentary basin, such as the Hontomín project (Alcalde et al., 2013) and the Sahagún and Los Páramos projects (Nardi et al., 2013).

There are four types of trapping mechanisms of $CO_2$ in a geological formation: structural-stratigraphic, residual, dissolution and mineral trapping (Bachu et al., 2007). Mineral trapping is important in long term, whereas the first three mechanisms dominate to short and medium terms. The rock microstructure plays an important role in the trapping of $CO_2$. Accurate knowledge of the microstructure is essential for determining the storage capacity and efficiency of $CO_2$ transport or retention for a rock, so studying the microstructure has become an essential working issue in research projects related to the geological storage of $CO_2$.

The work and the results presented in this article are part of the Pma$CO_2$ (Porosity and $CO_2$ trapping mechanisms) project. The aim of this project is the characterisation of the Utrillas porous system before and after $CO_2$ injection (1) to evaluate this system as a potential $CO_2$ storage formation, (2) to estimate the storage capacity of these systems and (3) to assess the retention mechanisms and changes after injection of $CO_2$. These changes in the pore space microstructure can not only significantly modify the storage capacity but also change the pattern and velocity of movement or the fluid through a rock. Thus, this work aims to contribute to the knowledge on the pore structure changes that take place after simulated injection.

## 2. Utrillas Sandstones

The Utrillas Sandstones Unit is a sedimentary siliciclastic formation whose age is located at the lower–upper limit of the Cretaceous. Consists of terrigenous material, conglomerates, sandstones and clays forming a macro sequence that includes several sequences with variable thicknesses. The stratigraphic macro sequence evolves from very coarse-grained sandstones, predominately at the bottom, and medium-grained and fine sandstones in the middle and upper part.

* Corresponding author. Tel.: +34 91 3466348.
*E-mail addresses:* rocio.campos@ciemat.es (R. Campos), iciar.barrios@ciemat.es (I. Barrios), javier.lillo@urjc.es (J. Lillo).

http://dx.doi.org/10.1016/j.egyr.2015.01.004

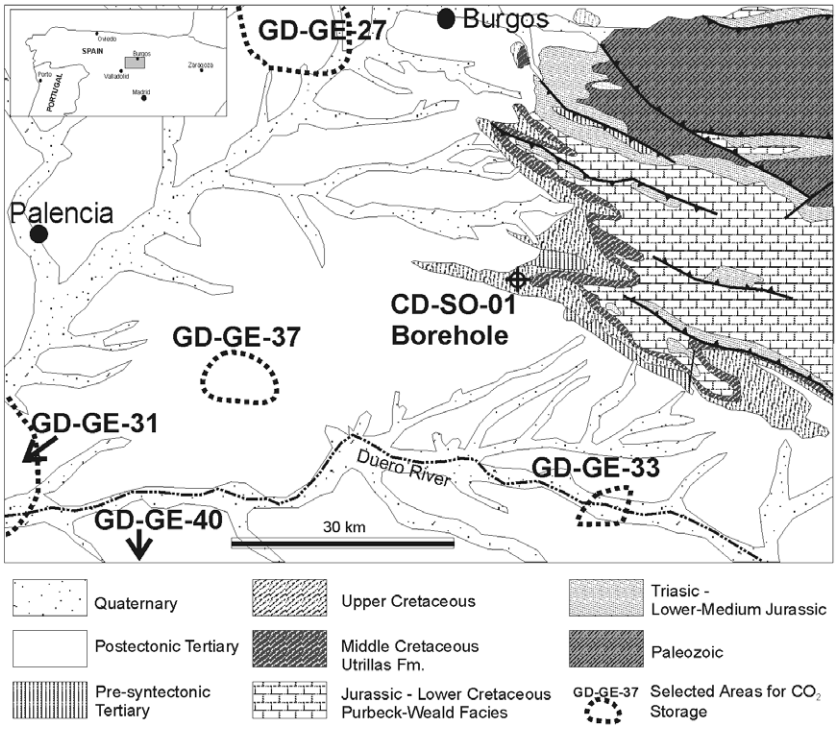


**Fig. 1.** Location of preselected areas for injection of $CO_2$ in the Duero Basin, where Utrillas Sandstones constitute the geologic storage formation. (1) CDGE-27, 1750 m depth–190 m thick (2) CDGE-31, 1170 m depth–40 m thick (3) CDGE-33, 1250 m depth–150 m thick (4) CDGE-37, 1300 m depth–140 m thick, and (5) CDGE-40 (outside of the graph), 950 m depth–50 m thick. Also shown is the position of the CD-SO-01 borehole in which sampling was performed.
*Source:* (Modified from IGME, 2010).

The lithological, structural and geometric characteristics of Utrillas Sandstones make it a favourable geological formation for $CO_2$ injection and storage. Fig. 1 shows the location of preselected areas for injection of $CO_2$ in the Duero Basin, where Utrillas Sandstones constitute the geologic storage formation. This work shows the study of the fine-medium grained sandstones sampled in the CD-S0-1 borehole (IGME, 2010).

The facies sampled at a depth of 35.4 m, studied with microscopic and MEB observations corresponds to a heterometric subarkose that is fine-medium grained, has a quartz–feldspathic composition, has a clay matrix and is variably cemented by carbonates. The dominant mineral fractions are quartz (> 79%) and feldspar (> 21%). Micas, rock fragments, rutile and ilmenite can be found at lesser frequencies. The matrix consists mainly of kaolinite and illite. There is an abundance of the cement calcareous.

## 3. Materials and methods

### 3.1. Materials

We have studied two samples M1 and M2. The M1 sample represents the original state of the rock before the injection and M2 represents the state after injection.

Both samples are from the same rock and they were separated a few millimetres in the borehole. We assume that variations between them are acceptable in average terms. To operate with those mean values were analysed six specimens from each sample and all results shown in this work for M1 and M2 are mean values.

### 3.2. $CO_2$ injection

The injection experiment was performed using a core sample (Fig. 2a) re-sized to a diameter of 38 mm and a length of 100 mm (Fig. 2b). The new sample was saturated in synthetic saline water (brine), before being put into the $CO_2$ injection cell.

**Table 1**
Water chemistry composition modelled with PHREEQC in equilibrium with the rock.

| | Concentration × $10^{-6}$ (kg/m$^3$) |
|---|---|
| $HCO_3^-$ | 543.54 |
| $Cl^-$ | 17.68 |
| $SO_4^{2-}$ | 1.64 |
| $Ca^{2+}$ | 32.1 |
| $Mg^{2+}$ | 12.23 |
| $K^+$ | 201.86 |
| $Na^+$ | 21.16 |
| $SiO_2$ | 12.06 |

The synthetic water was prepared specifically for this experiment by IMDEA-Agua. The hydrogeochemical code PHREEQC, developed by the U.S. Geological Survey (USGS), was used to model the water chemistry. This code allows us to establish the compositional pattern of a particular equilibrium solution with the mineral phase constituents of a solid reactive phase (Parkhurst and Appelo, 1999; Parkhurst et al., 2013). As an initial solution to model, we considered a representative composition of a groundwater typical of an aquifer in detrital materials with a quartz–feldspar composition. We set a pH of 7.68 and a temperature of 32 °C, which is the same as the set temperature for the $CO_2$ test injection.

The chemical composition of this water in equilibrium with the formation is summarised in Table 1.

To carry out the experiment, a thermo-resistant cover was put on the dry sample (Fig. 2c). Then, both were put inside a Viton cylinder (Fig. 2d) with high elasticity, high resistance to aggressive fluids and high temperatures. After that, the sample in the Viton was placed inside the injection cell (Fig. 2e). The injection cell was built for this type of test for the Petrophysical Institute Foundation, with which we have collaborated on the project. The patented reference number of the equipment is P201231913 IPf-UPM.

The low permeability of the sample (2.57 $10^{-16}$ m$^2$) made the injection flow very low and it took place over several days to reach

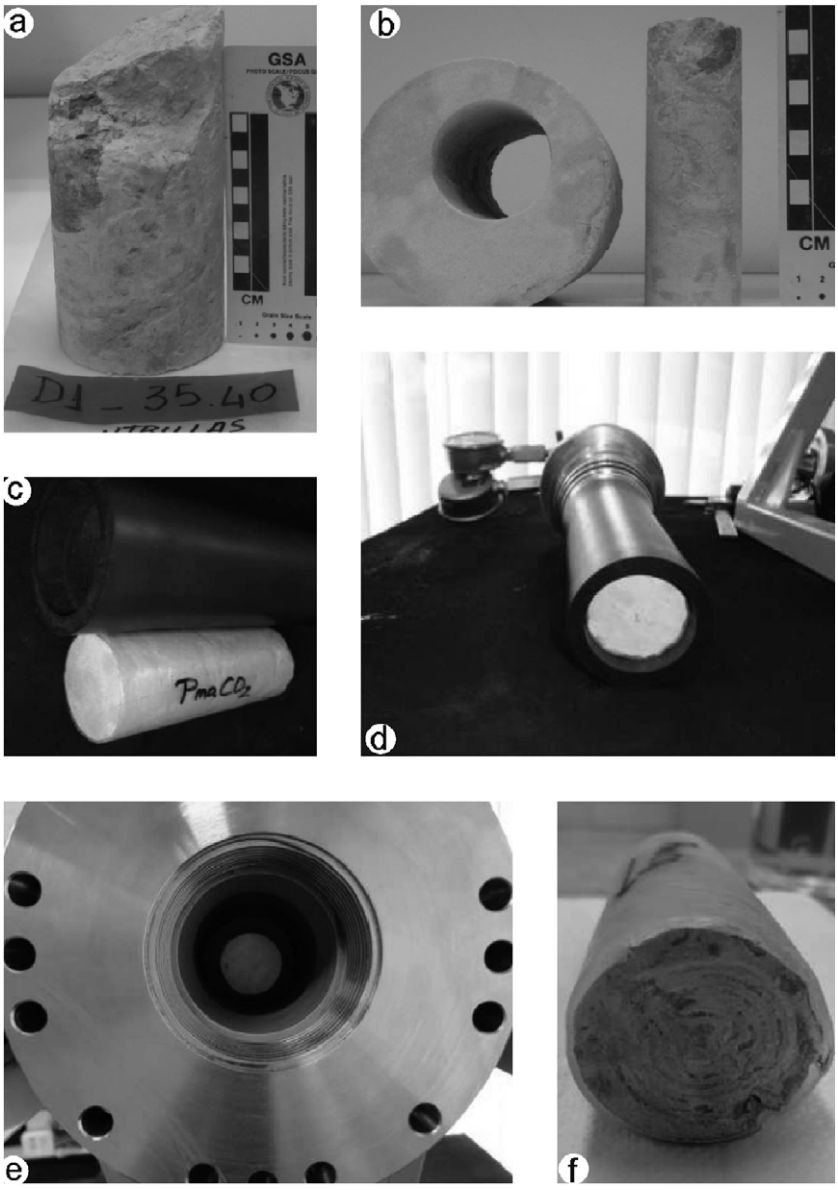


**Fig. 2.** (a) Borehole core, (b) 38 mm-diameter core sample, (c) core sample in thermo-retractable plastic cover, (d) core sample in Viton, (e) core sample in injection chamber and, (f) core sample after experimental injection.

saturation. The saturation is considered to be completed when there are no variations in the weight of the sample. Once the sample was saturated with the brine, the cell was connected to a generator of supercritical carbon dioxide ($CO_2$sc), with the injection and evacuation or production valves opened; thus, displacement of the brine due to the injection of $CO_2$ was simulated. The evacuation valve was connected to a phase separator that registers both water production and $CO_2$ production. At 330 min from the beginning of the injection, the production of $CO_2$ did not reach the outlet valve, and, after 1226 min, the brine production became undetectable. At this moment, the sample was considered saturated with $CO_2$ along with the non-reducible salt water (or irreducible brine). Injection pressure during the experiment varied between 7 and 12 MPa.

Once the sample with $CO_2$sc was saturated, the cell remained closed for two months, with the pressure (8 MPa) and temperature conditions (32 °C) controlled daily. At the end of the test, after 60 days, the confining pressures were reduced, the valves were opened, the Viton was removed and the sample was collected in perfect condition (Fig. 2f).

### 3.3. Hg porosimetry

Characterising the pores includes the determination of the total pore volume, the pore size distribution and the study of their morphology and connectivity. Mercury Intrusion Porosimetry (MIP) analysis was carried out with the Autopore IV 9500, using the mercury filling at pressures from 0.0026 MPa to 219.9251 MPa permitting to characterise the pore diameter from 276793 nm to 3.3 nm calculated by the Washburn equation (Washburn, 1921). The experimental measurements follow the ASTMD4404 — 10 standard (2010).

MIP provides data related to the features of the pore space and related to the different physical properties of the material (Webb, 2001). The parameters determined are (1) the total intruded Hg volume in $m^3/kg$; (2) the total pore area in $m^2/kg$; (3) the average pore radius in micrometres; (4) the porosity in %; (5) the threshold pressure, which is the pressure from which the fluid percolates through the sample; (6) the characteristic length corresponding to the pressure threshold; and (7) the tortuosity .

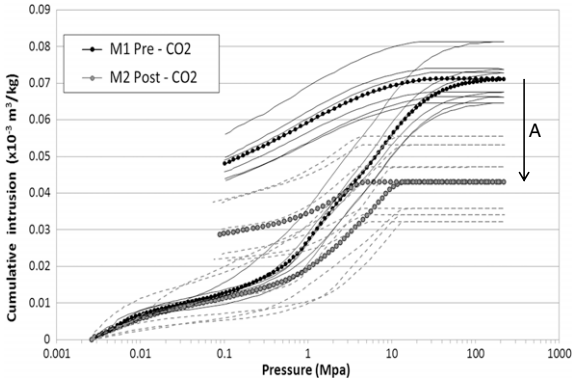


**Fig. 3.** Intrusion–extrusion curves for the M1 and M2 samples (six specimen of each sample). Thick lines represent the mean values. (A) Represents the difference in the total volume of intruded mercury between M1 and M2, is the difference in the porosity between M1 and M2.

We use the International Union of Pure and Applied Chemistry (IUPAC) classification for pore size based on the Boucher classification (Boucher, 1976): (1) macropores have diameters $> 50$ nm, (2) mesopores, between 2 nm and 50 nm, and (3) micropores $< 2$ nm.

Porosimetry determinations were carried out on two samples M1 (pre$CO_2$) and M2 (post$CO_2$). Six specimens were measured in each sample and mean values were determined.

### 3.4. Pore network modelling

The porous system model in the reservoir rocks represents a challenge in the research on geological $CO_2$ storage. Modelling the characteristics of the porous system that includes the hydraulic behaviour of the rock to matrix-scale, is critical in understanding how the mechanisms of trapping actuate.

Usually, the models used for the interpretation of mercury porosimetry curves are too simplistic and do not provide realistic results on the structure of materials, their pores and their connections. The tool used in this work is the PoreCor© software, which models the pore structure using Hg porosimetry curves. It was developed by the Environmental and Fluid Modelling Group of the Plymouth University in England. PoreCor© can generate quasi-realistic models, and it has been used by various authors for modelling different materials such as soil, rock, membranes and paper (Johnson et al., 2003; Matthews et al., 1995a,b, 2006). It has also been used to simulate diffusion processes (Laudone et al., 2008) or absorption (Ridgway and Gane, 2002) through a porous structure. In this work, we use PoreCor© as a tool for comparison between the microstructure of Utrillas Sandstones before and after $CO_2$ supercritical ($CO_2$sc) injection.

PoreCor© represents the void structure of a porous medium as a series of identical interconnected unit cells. Each unit cell comprises an array of 1000 nodes regularly distributed in a cartesian cubic space. The pores are numbered from left to right, from front to back, and from bottom to top and are represented as cubes. Cubic pores are positioned with their centres at each node and connected by smaller cylindrical pores oriented in the three Cartesian directions (Laudone et al., 2008). The types of structures that PoreCor© can generate are: random representing a disordered structure, horizontally banded with pores ranging from fine to coarse vertically, pores varying towards the centre, vertically banded pores, or a radial structure with two variations, coarse to fine towards the centre or fine to coarse towards the centre (Laudone et al., 2008). The type of structure to be applied in the model and the variation of the correlation coefficient are the first decisions to make in the modelling process.

The effects of the $CO_2$sc injection on the pore structure in Utrillas Sandstones were studied from the models generated

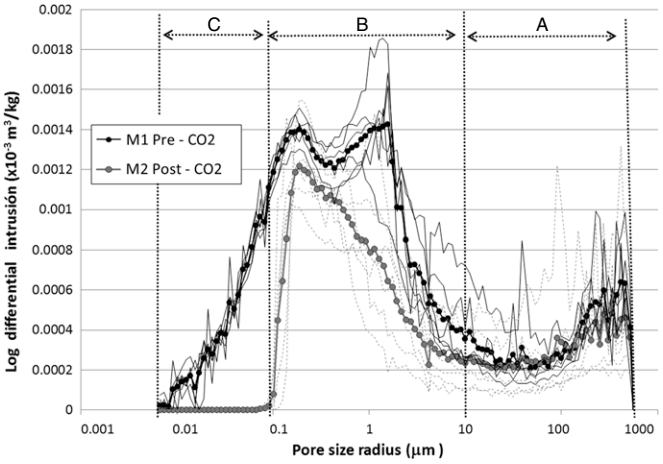


**Fig. 4.** Mean pore diameter distribution curves obtained from MIP in samples M1 and M2 (six specimen of each sample). The zones (A), (B) and (C) are associated with the selective decrease in porosity explained in the text.

in PoreCor©. For each sample (M1 pre-injection and M2 post-injection), modelling was carried out in 6 specimens.

For this work, we chose a horizontally banded pore structure, but we imposed high permissiveness in adjustment of the correlation coefficient. In this way, we do not limit the random tendency in the arranged pores and throats. The resulting configurations represent a banded structure with randomly arranged pores and throats.

The first and major advantage of these models is that we can differentiate between pores and pore connections (throats) with smaller dimensions. It is possible to simulate structures with large pores surrounded by narrow connections similar to bottleneck pores, which are very common in geological materials and produce hysteresis, such as that observed in the Hg intrusion–extrusion curves (Fig. 3).

The parameters that have been used for modelling (Table 3) are (1) the pore coordination number, which is the number of connections of a pore with adjacent pores; (2) connectivity, which is the average of the pore coordination numbers; (3) pore skew, which is a parameter that bulks up the pores to obtain the correct porosity; and (4) the throat skew, which controls the throat size distribution in collaboration with the (5) throat spread, which increases the throat size distribution. With these parameters, the fitting of the model to the experimental porosity is done by (a) altering the spacing between the nodes, (b) altering the lengths of the throats leading to an approach or spacing between pores, (c) varying the size of the pores and/or (d) adjusting the radius of the cylinder representing the throats (Matthews et al., 1995a,b, 2006). The results are shown in Table 3.

Optimisation of the adjustment function is performed using a local geometric algorithm, the Simplex Method (Nelder and Mead, 1965), combined with a stochastic global optimisation method, Simulated Annealing (Johnson et al., 2003).

## 4. Results

The results of the determinations performed on the six specimens from each sample and the average values are summarised in Table 2. This table also shows the differences in % between the mean M1 and M2 values. The average intrusion–extrusion curves and the pore size distributions are shown in Figs. 3 and 4.

Some differences between M1 and M2 may be observed. The total volume of intruded mercury, which is the parameter that gives an idea of the capacity of the rock, decreases from 0.071 $10^{-3}$ $m^3$/kg in M1 to 0.043 $10^{-3}$ $m^3$/kg in M2. These values are at the maximum test pressure. This change represents a decrease

**Table 2**
Parameters obtained from the mercury intrusion porosimetry on the six specimens from each sample (M1 and M2), medium values (Averg.) and differences between M1 and M2 medium values (Diff. M1 – M2 (%)).

| Sample | Spc. | Total Intrs. Vol. $\times 10^{-3}$ ($m^3$/kg) | Total Pore Area $\times 10^3$ ($m^2$/Kg) | Median Pore Radius (Volume-μm) | Median Pore Radius (Area-μm) | Average Pore Radius (2V/A) (μm) | Porosity (%) | Charact. length (μm) | Tortuosity |
|---|---|---|---|---|---|---|---|---|---|
| M1 pre $CO_2$ | 1 | 0.0728 | 1.79 | 0.40 | 0.02 | 0.08 | 15.93 | 168.46 | 7.30 |
| | 2 | 0.0675 | 1.54 | 0.41 | 0.02 | 0.09 | 15.02 | 209.03 | 6.96 |
| | 3 | 0.0737 | 1.52 | 0.39 | 0.03 | 0.10 | 16.10 | 138.27 | 9.03 |
| | 4 | 0.0661 | 1.71 | 0.28 | 0.02 | 0.08 | 14.76 | 190.55 | 8.53 |
| | 5 | 0.0646 | 1.56 | 0.30 | 0.02 | 0.08 | 14.49 | 164.35 | 7.34 |
| | 6 | 0.0813 | 1.50 | 0.51 | 0.03 | 0.11 | 17.55 | 191.47 | 8.02 |
| | Averg. | 0.0710 | 1.60 | 0.38 | 0.03 | 0.09 | 15.64 | 177.02 | 7.86 |
| M2 post $CO_2$ | 1 | 0.0555 | 0.29 | 1.16 | 0.13 | 0.38 | 12.24 | 233.20 | 3.78 |
| | 2 | 0.0341 | 0.33 | 0.28 | 0.11 | 0.21 | 7.88 | 222.50 | 4.32 |
| | 3 | 0.0358 | 0.30 | 0.48 | 0.10 | 0.24 | 8.28 | 209.91 | 4.21 |
| | 4 | 0.0531 | 0.31 | 1.78 | 0.11 | 0.35 | 11.73 | 167.36 | 4.64 |
| | 5 | 0.0475 | 0.51 | 0.50 | 0.09 | 0.19 | 10.56 | 190.11 | 4.05 |
| | 6 | 0.0322 | 0.35 | 0.25 | 0.09 | 0.19 | 7.49 | 164.73 | 4.49 |
| | Averg. | 0.0430 | 0.35 | 0.74 | 0.11 | 0.26 | 9.70 | 197.97 | 4.25 |
| Diff. | M1 – M2 (%) | −39 | −78 | 48 | 76 | 65 | −38 | 10 | −46 |

of 39% in the total intruded volume. Fig. 3 shows these variations in the height of the Hg intrusion curves. As expected, the porosity decreases in a similar way, with a reduction of 38% between the M1 and M2 samples (e.g., before and after the injection of $CO_2$), from 15.64% to 9.70%.

The total pore area also decreases from 1.60 $10^{-3}$ $m^2$/kg to 0.35 $10^{-3}$ $m^2$/kg. This very high reduction in the total area of pores, 78%, is interpreted as being due to a *selective* reduction of porosity. The porosity decreases include the complete disappearance of the mesoporosity and a reduction in the macroporosity.

There are three zones in the pore size distribution curve (Fig. 4). In Zone A, the pore size distributions in M1 and M2 are very similar and correspond to pores with radii greater than 7 μm. The pore size distribution in this area does not vary by injection of $CO_2$. In Zone B, with pore radii between 0.041 and 7 μm, the distribution of pores in M2 is different from M1. Within this area, the smaller pores decrease, and the porosity decreases with $CO_2$ injection. Finally, Zone C (Fig. 4), which represents the pores with radii of less than 0.041 μm, disappears completely in sample M2. $CO_2$ injection and associated reactions cause the disappearance of part of the mesoporosity and macroporosity.

The average pore radius and the characteristic length are greater in M2 (Table 2) due to the elimination of the mesoporosity.

Mineral precipitation was studied by Pruess and Müller (2009), who show that the injection of $CO_2$ into saline aquifers may cause a dry-out formation and the precipitation of salt near the injection well, which may reduce the formation of porosity, permeability, and injectivity. Recently, Ellis and Bazylak (2013a,b) show that this precipitation may significantly reduce the injection rock's permeability to $CO_2$ penetration, which could compromise the $CO_2$ injection process. According to Alkan et al. (2010), higher salinity and capillary pressure can even block the pores, causing increased salt precipitation, and according to Rad et al. (2013) the salt precipitation patterns (in drying experiments) are nonuniform, they show the important influence of the pore size distribution in the dynamics of salt crystallisation.

Tortuosity defined as the ratio of the distance between two points, including any curves encountered, divided by the straight line distance, decreases in sample M2. After the injection of $CO_2$, as the porosity decreases, the efficiency of the transfer of fluid through the porous rock can increase because the pathways are less tortuous.

Finally, we must remark that hysteresis or mismatch between the intrusion and extrusion curves (Fig. 3) indicates the existence of porosity trapped in cavities connected by bottleneck-shaped pores. This shape decreases connectivity and transport efficiency. In both the M1 and M2 samples, there is a high percentage of entrapped porosity, where Hg is irreversibly trapped in the porous structure.

The results from the twelve specimens modelled by PoreCor© are shown in Table 3, which summarises the principal parameters as well as the mean values. Modelling was carried out in each case starting from a horizontally banded structure with throats with cylindrical geometry and a free correlation coefficient.

The mean distance (Table 3) between the simulated and experimental models, 1.34 and 1.63 for M1 and M2 respectively, indicates a good degree of adjustment. The level of correlation between the model and the resultant banding model in each specimen is very low (Table 3), indicating a random organisation of pores and throats in the unit cell. In several specimens, the correlation level is so low that we can ensure a random arrangement of pores.

Differences between M1 and M2 are evident in the pore spacing and, consequently, the size of the unit cell. The pore spacing increases in sample M2, indicating a lower density of pores per unit volume. However, the connectivity between pores is almost the same in the two samples. The average values (3.37 and 3.51) indicate high connectivity.

Fig. 5 shows the graphical results of the modelling of one of the specimens: (a) the fit between the experimental and simulated curves, (b) the 3D network of pores and throats modelled in the unit cell and (c) the same network representation with solid particles modelled as spheres. Regardless of the real morphology of the particles, the particle size distribution is calculated using the mathematical model proposed by Pospìch and Schneirder (1989).

In the generated models, the conditions under which percolation occurs and the differences between the pre-injected sample M1 and post-injected M2 are also studied (Table 3). In each case, the pressure required to produce percolation is 1064.67 kPa in M1 and 1897.61 kPa in M2. Thus, it is more difficult to drive fluid through the M2 rock. This effect is a direct consequence of the decreased porosity, despite the decreasing tortuosity experimentally determined in M2.

The pore space intruded by Hg at different pressures between 10 and 100 000 kPa and under a confining pressure of 7380 kPa is also studied (Fig. 6). The pressure of 7380 kPa represents the pressure at which $CO_2$ is in a supercritical state under a temperature of 31.1 °C. We note that a significant portion of pores will not be intruded by Hg under a confining pressure close to the critical pressure of $CO_2$. The rock would only be completely intruded by Hg at a very high pressure close to 100 MPa.

**Table 3**
Modelling parameters for the 12 specimens (samples M1 and M2) and average values for each sample. Porosity values are corrected for the compression of mercury, expansion of the penetrometer and compressibility of the sample.

| Samp. | Spc. | Exp. Porosity (%) | Distance between simul-expt | Correl. level | Pore row spacing (μm) | Unit cell size (μm) | Conec-tivity | Throat Skew | Throat Spread | Pore Skew | Percolation | | | |
|---|---|---|---|---|---|---|---|---|---|---|---|---|---|---|
| | | | | | | | | | | | at pore n° | at pore diameter (mm) | at intr. volume (%) | at press. (kPa) |
| M1 pre $CO_2$ | 1 | 15.89 | 1.52 | 0.08 | 923.5 | 9234.7 | 3.42 | −8.00 | 0.94 | 3.61 | 8 | 1.62 | 36.27 | 905.6 |
| | 2 | 13.34 | 1.33 | 0.06 | 903.5 | 9034.8 | 3.41 | −5.70 | 0.96 | 1.36 | 22 | 1.62 | 37.66 | 905.2 |
| | 3 | 15.28 | 1.24 | 0.09 | 929.5 | 9294.8 | 3.41 | −29.44 | 0.94 | 3.55 | 22 | 1.45 | 42.96 | 1016.5 |
| | 4 | 13.39 | 1.38 | 0.09 | 958.7 | 9586.6 | 3.41 | −29.34 | 0.98 | 2.40 | 22 | 1.29 | 41.61 | 1141.2 |
| | 5 | 14.21 | 1.25 | 0.10 | 954.2 | 9542.2 | 3.44 | −1.01 | 0.95 | 3.32 | 8 | 1.28 | 36.99 | 1142.7 |
| | 6 | 15.11 | 1.30 | 0.31 | 822.5 | 8224.7 | 3.14 | −26.27 | 0.73 | 2.77 | 13 | 1.15 | 51.69 | 1276.8 |
| | Averg. | 14.54 | 1.34 | 0.12 | 915.3 | 9153.0 | 3.37 | −16.63 | 0.92 | 2.83 | – | 1.40 | 41.20 | 1064.7 |
| M2 post $CO_2$ | 1 | 11.01 | 1.86 | 0.10 | 911.7 | 9117.3 | 3.84 | 0.00 | 0.92 | 1.01 | 26 | 1.44 | 51.19 | 1019.1 |
| | 2 | 6.94 | 1.39 | 0.01 | 1152.1 | 11521.0 | 3.44 | −33.64 | 0.85 | 2.02 | 8 | 1.02 | 35.80 | 1438.1 |
| | 3 | 6.94 | 1.57 | 0.01 | 1258.2 | 12582.0 | 3.45 | −20.49 | 0.83 | 4.32 | 94 | 0.46 | 63.23 | 3198.9 |
| | 4 | 11.04 | 1.52 | 0.27 | 984.2 | 9841.7 | 3.43 | 14.48 | 0.68 | 4.38 | 11 | 0.73 | 60.64 | 2025.3 |
| | 5 | 8.89 | 1.62 | 0.12 | 876.4 | 8763.9 | 3.26 | −27.95 | 0.73 | 1.26 | 82 | 1.02 | 49.01 | 1434.7 |
| | 6 | 4.86 | 1.83 | 0.11 | 1370.5 | 13705.0 | 3.64 | −49.49 | 0.71 | 1.38 | 22 | 0.65 | 50.13 | 2269.7 |
| | Averg. | 8.28 | 1.63 | 0.10 | 1092.2 | 10921.8 | 3.51 | −19.52 | 0.79 | 2.40 | – | 0.89 | 51.67 | 1897.6 |

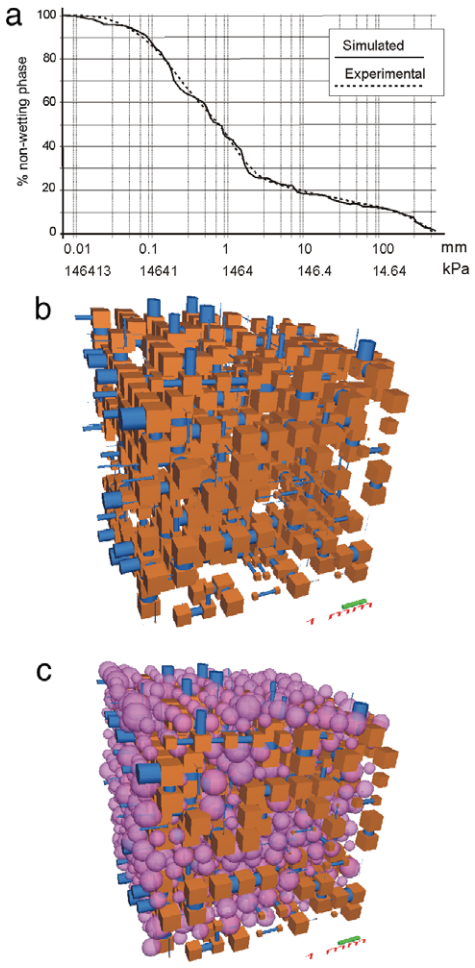


**Fig. 5.** Modelling results for M1(specimen-3): (a) fit between simulated and experimental curves, (b) three-dimensional representation of pores and throats in unit cell, and (c) three-dimensional structural representation with particles.

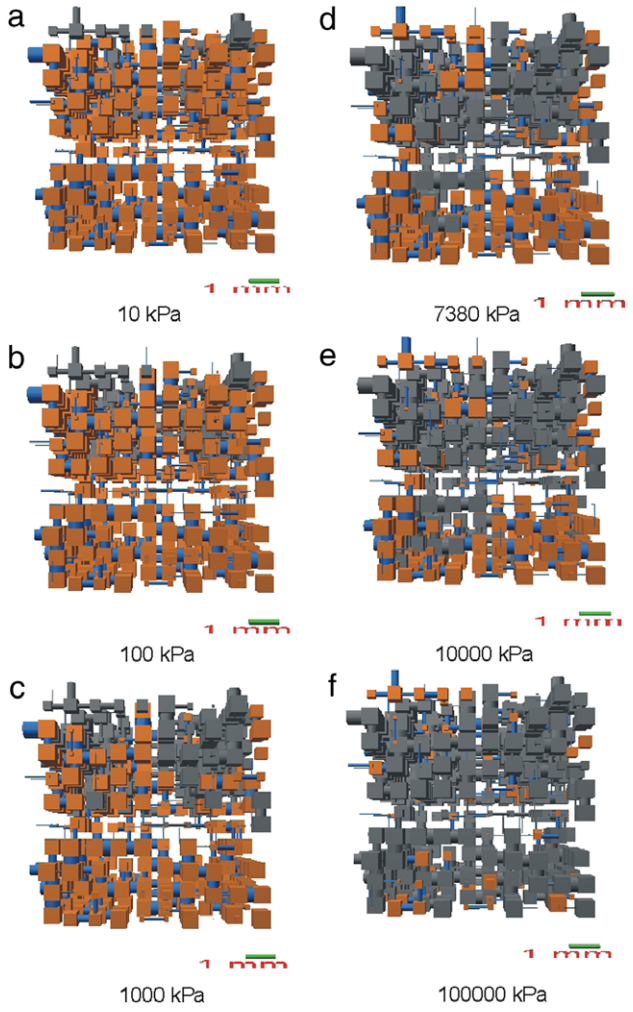


**Fig. 6.** Simulated Hg flow through the unit cell at different injection pressures between 10 and 100 000 kPa.

## 5. Discussion

Geological $CO_2$ storage in deep saline detrital (siliciclastic) aquifers is a promising option to mitigate global warming, and the Duero Basin in NW Spain is one of the most promising basins for $CO_2$ storage in the Iberian Peninsula. However, precise knowledge of the microstructure of the reservoir rock is essential for determining the storage capacity, transport efficiency and retention of $CO_2$. In this study, we present results regarding variations in the pore space of the fine-medium grained sandstones rocks of the Utrillas Formation caused by the injection of $CO_2$sc and its permanence in supercritical conditions in contact with the rock sample for two months.

$CO_2$sc injection was performed in a static test, keeping the sample in the cell for 60 days under storage pressure and temperature conditions. This type of static test could serve as a complement to dynamic tests, such as those from Wigand et al. (2008) or studies performed for demonstration projects (Eiken et al., 2011; Pawar et al., 2006; Hovorka et al., 2006).

The static tests of $CO_2$ injection in the laboratory contribute to our understanding of the dynamics of the gas in the formation after a period from the start of injection as a complement to the dynamic tests focused on studying of the effects of $CO_2$ flow. The static test allows us to tackle knowledge of the long-term physical (and chemical) changes that will take place in the formation.

From the mercury intrusion–extrusion curves and the pore space modelling after the $CO_2$ injection experiment, we observe significant changes in the pore space. These variations may not only alter the storage capacity but also change the pattern of $CO_2$ flow or percolation through a rock.

As a consequence of a $CO_2$ residence time of two months in the rock, a drastic reduction of porosity occurs in the rock. In addition, the volume of the intruded mercury – as determined by MIP – decreases at a high percentage. This decrease demonstrates the significant impact that $CO_2$ injection has on the storage capacity of the rock.

The prominent decrease in the total pore area – another parameter estimated by MIP – could be an evidence of a selective porosity reduction affecting mainly the mesoporosity and, to a lesser extent, the macroporosity. The mesoporosity of the rock disappears with the $CO_2$sc injection, and the macroporosity decreases. Currently, we are obtaining preliminary results from geochemical analysis and differential thermal and thermogravimetric analyses that suggest that the mesoporosity disappearance is caused by mineral precipitation in pores of smaller size by $CO_2$sc-brine reaction.

Mineral precipitation in the injection of $CO_2$ into saline aquifers may cause salt precipitation, which may reduce the porosity, permeability, and injectivity of the formation. Our work demonstrates that the $CO_2$sc sequestration by neoformation and mineral precipitation occurs within a much shorter time than has yet been considered.

Due to the disappearance of the smaller pores, the tortuosity of the injected sample decreases. This phenomenon may contribute in a positive way to the efficient transfer of fluid through the rock;

however, the decrease in porosity is so high in this case that this increase in the efficiency by reducing the tortuosity is minimised.

With the MIP results, we have modelled the samples pre- and post-injection. Although the generated structures are not entirely realistic, they represent a good approximation of the geometry of the pores. The structures are isotropic and, although they have a very slight banding component, present an arrangement of random pores and throats.

The 3D geometric models – which were generated from the MIP – have been used to extract the pore space network and its complementary grain matrix network and to quantitatively characterise the architecture and geometry of the pore network.

The Hg flow simulation work carried out for different pore geometries and for different pressures shows that the methodology is suitable for the study of $CO_2$sc flows through a rock; it is this aspect on which we are currently focusing our work. Thus, in future works, we will investigate the intrusion of supercritical $CO_2$ within these networks.

As a result of the comparative analysis of the pore network geometry, it is concluded that the percolation threshold pressure after injection is greater as a result of the decreasing porosity.

## 6. Conclusions

A static test of $CO_2$ injection on an Utrillas sample in a synthetic brine was performed to reproduce the storage conditions after $CO_2$ injection in the geological formation.

After the test, significant changes in the pore space were found, which in turn produce variations in the storage capacity and the pattern of $CO_2$ flow through the rock.

The observed reduction of porosity affects drastically to a large volume of pore space, but in a selective way, mainly to mesopores. The most plausible cause for the mesoporosity loss is mineral precipitation in the pores of smaller size.

The reduction of porosity, and subsequently, the reduction of the effective storage capacity after $CO_2$ injection must be taken into account in the assessment of the potential formations for geological $CO_2$ storage.

## Acknowledgements

This work has been carried out under the PmaCO2 - CGL2011-24768 project funded by Ministry of Economy and Competitiveness of Spain. The authors would like to thank I. Suárez, Geological and Mining Institute of Spain (IGME), for their facilities, access to information and core sampling. We also thank to Madrid Institute for Advanced Studies — Water (IMDEA), especially to M. Leal for collaboration in the modelling of water chemistry and the production of synthetic water. The injection tests were completed in the laboratories of the Institute Foundation Petrophysical (IPf), and the petrophysical analysis was performed in the Petrophysics Laboratory of Research Center in Energy, Environment and Technology (CIEMAT). We especially thank A.M. González for the dedication and contributions in these works. Comments and suggestion from anonymous reviewer improved this manuscript.

## References

Alcalde, J., Martí, D., Calahorrano, A., Marzan, I., Ayarza, P., Carbonell, R., Juhlin, C., Pérez-Estaún, A., 2013. Active seismic characterization experiments of the Hontomín research facility for geological storage of $CO_2$, Spain. Int. J. Greenh. Gas Control (ISSN: 1750-5836) 19, 785–795. http://dx.doi.org/10.1016/j.ijggc.2013.01.039.

Alkan, H., Cinar, Y., Ülker, E.B., 2010. Impact of capillary pressure, salinity and in situ conditions on $CO_2$ injection into saline aquifers. Transp. Porous Media 84 (3), 799–819. http://dx.doi.org/10.1007/s11242-010-9541-8.

ASTMD4404, Standard Test Method for Determination of Pore Volume and Pore Volume Distribution of Soil and Rock by Mercury Intrusion Porosimetry. http://dx.doi.org/10.1520/D4404-10, http://www.astm.org/Standards/D4404.htm.

Bachu, S., Bonijoly, D., Bradshaw, J., Burruss, R., Holloway, S., Christensen, N.P., Mathiassen, O.M., 2007. $CO_2$ storage capacity estimation: Methodology and gaps. Int. J. Greenh. Gas Control (ISSN: 1750-5836) 1 (4), 430–443. http://dx.doi.org/10.1016/S1750-5836(07)00086-2.

Boucher, E.A., 1976. Porous materials: structure, properties and capillary phenomena. J. Mater. Sci. 11 (9), 1734–1750. http://dx.doi.org/10.1007/BF00737529.

Eiken, O., Ringrose, P., Hermanrud, C., Nazarian, B., Torp, T.A., Høier, L., 2011. Lessons learned from 14 years of CCS operations: Sleipner, In Salah and Snøhvit. Energy Procedia (ISSN: 1876-6102) 4 (0), 5541–5548. http://dx.doi.org/10.1016/j.egypro.2011.02.541.

Ellis, J.S., Bazylak, A., (2013a). $CO_2$–brine solubility and the effects of salt precipitation during carbon dioxide injection through pore-scale network modeling. Abstract 1383, 223rd ECS Meeting. The Electrochemical Society Meeting, Toronto. http://ma.ecsdl.org/content/MA2013-01/40/1383.full.pdf.

Ellis, J.S., Bazylak, A., 2013b. Investigation of contact angle heterogeneity on $CO_2$ saturation in brine-filled porous media using 3D pore network models. Energy Convers. Manage. (ISSN: 0196-8904) 68 (0), 253–259. http://dx.doi.org/10.1016/j.enconman.2013.01.019.

Hovorka, S.D., Benson, S.M., Doughty, C., Freifeld, B.M., Sakurai, S., Daley, T.M., Kharaka, Y.K., Holtz, M.H., Trautz, R.C., Nance, H.S., Myer, L.R., Knauss, K.G., 2006. Measuring permanence of $CO_2$ storage in saline formations: the Frio experiment. Environ. Geosci. 13 (2), 105–121 , http://archives.datapages.com/data/deg/2006/EG05011/EG05011.htm?doi=10.1306%2Feg.11210505011.

IGME, 2010. Selection and characterization of geological structures and favourable areas for geological storage of $CO_2$. http://www.igme.es/infoigme/aplicaciones/algeco2.

Johnson, A., Roy, I.M., Matthews, G.P., Patel, D., 2003. An improved simulation of void structure, water retention and hydraulic conductivity in soil with the Pore-Cor three-dimensional network. European J. Soil Sci. 54 (3), 477–490. http://dx.doi.org/10.1046/j.1365-2389.2003.00504.x, http://onlinelibrary.wiley.com/doi/10.1046/j.1365-2389.2003.00504.x/abstract.

Laudone, G.M., Matthews, G.P., Gane, P.A.C., 2008. Modelling diffusion from simulated porous structures. Chem. Eng. Sci. (ISSN: 0009-2509) 63 (7), 1987–1996. http://dx.doi.org/10.1016/j.ces.2007.12.031.

Matthews, G.P., Canonville, C.F., Moss, A.K., 2006. Use of a void network model to correlate porosity, mercury porosimetry, thin section, absolute permeability, and NMR relaxation time data for sandstone rocks. Phys. Rev. E. 73 (3), 031307. http://dx.doi.org/10.1103/PhysRevE.73.031307.

Matthews, G.P., Moss, A.K., Ridgway, C.J., 1995a. The effects of correlated networks on mercury intrusion simulations and permeabilities of sandstone and other porous media. Powder Technol. (ISSN: 0032-5910) 83 (1), 61–77. http://dx.doi.org/10.1016/0032-5910(94)02942-H.

Matthews, G.P., Ridgway, C.J., Spearing, M.C., 1995b. Void space modeling of mercury intrusion hysteresis in sandstone, paper coating, and other porous media. J. Colloid Interface Sci. (ISSN: 0021-9797) 171 (1), 8–27. http://dx.doi.org/10.1006/jcis.1995.1146.

Nardi, A., Grandia, F., Abarca, E., Motis, K., Molinero, J., 2013. Model quantification of the $CO_2$ storage in the Los Páramos site (Duero basin, NE Spain), Geophysical Research Abstracts 15, EGU2013-7625, EGU General Assembly. http://adsabs.harvard.edu/abs/2013EGUGA..15.7625N.

Nelder, J.A., Mead, R., 1965. A Simplex method for function minimization. Comput. J. 7 (4), 308–313. http://dx.doi.org/10.1093/comjnl/7.4.308.

Pacala, S., Socolow, R., 2004. Stabilization Wedges: Solving the Climate Problem for the Next 50 Years with Current Technologies. Science 305 (5686), 968–972. http://dx.doi.org/10.1126/science.1100103, https://www.sciencemag.org/content/305/5686/968?related-urls=yes&legid=sci;305/5686/968.

Parkhurst, D.L., Appelo, C.A.J., 1999. User's guide to PHREEQC (version 2) – A computer program for speciation, batch-reaction, one-dimensional transport, and inverse geochemical calculations: U.S. Geological Survey Water-Resources Investigations Rep. 99-4259, 312p.

Parkhurst, D.L., Appelo, C.A.J., Parkhurst, D.L., Appelo, C.A.J., 2013, Description of input and examples for PHREEQC version 3A computer program for speciation, batch-reaction, one-dimensional transport, and inverse geochemical calculations. U.S. Geological Survey Techniques and Methods 6(A43), 497p. http://pubs.usgs.gov/tm/06/a43/.

Pawar, R.J., Warpinski, N.R., Lorenz, J.C., Benson, R.D., Grigg, R.B., Stubbs, B.A., Stauffer, P.H., Krumhansl, J.L., Cooper, S.P., Svec, R.K., 2006. Overview of a $CO_2$ sequestration field test in the West Pearl Queen reservoir, New Mexico. Environ. Geosci. 13 (3), 163–180. http://dx.doi.org/10.1306/eg.10290505013, http://baervan.nmt.edu/groups/gas-flooding/publications/co2sequestration/p-10.html.

Pospìch, R., Schneirder, P., 1989. Powder particle sizes from mercury porosimet. Powder Technol. (ISSN: 0032-5910) 59 (3), 163–171. http://dx.doi.org/10.1016/0032-5910(89)80062-2.

Pruess, K., Müller, N., 2009. Formation dry-out from $CO_2$ injection into saline aquifers: 1. Effects of solids precipitation and their mitigation. Water Resour. Res. 45, W03402. http://dx.doi.org/10.1029/2008WR007101, http://onlinelibrary.wiley.com/doi/10.1029/2008WR007101/abstract.

Rad, M.N., Shokri, N., Sahimi, M., 2013. Pore-scale dynamics of salt precipitation in drying porous media. Phys. Rev. E 88, 032404-1-5. http://dx.doi.org/10.1103/PhysRevE.88.032404, http://link.aps.org/doi/10.1103/PhysRevE.88.032404.

Ridgway, C.J., Gane, P.A.C., 2002. Dynamic absorption into simulated porous structures. Colloids Surf. A (ISSN: 0927-7757) 206 (1–3), 217–239. http://dx.doi.org/10.1016/S0927-7757(02)00078-X.

Washburn, E.W., 1921. The dynamics of capillary flow. Phys. Rev. 17, 273–283. http://dx.doi.org/10.1103/PhysRev.17.273.

Webb, P.A., 2001. An introduction to the physical characterization of materials by mercury intrusion porosimetry with emphasis on reduction and presentation of experimental data, Micromeritics Instrument© USA. 23p. http://www.micromeritics.com/pdf/app_articles/mercury_paper.pdf.

Wigand, M., Carey, J.W., Schütt, H., Spangenberg, E., Erzinger, J., 2008. Geochemical effects of $CO_2$ sequestration in sandstones under simulated in situ conditions of deep saline aquifers. Appl. Geochem. (ISSN: 0883-2927) 23 (9), 2735–2745. http://dx.doi.org/10.1016/j.apgeochem.2008.06.006.